Journal of Chromatography, 559 (1991) 257–266
Elsevier Science Publishers B.V., Amsterdam

CHROM. 23 459

Capillary electrophoresis of DNA in entangled polymer solutions

PAUL D. GROSSMAN* and DAVID S. SOANE
Department of Chemical Engineering, University of California at Berkeley, Berkeley, CA 94720 (USA)

ABSTRACT

Electrophoretic separations of DNA restriction fragments were performed in solutions of hydroxyethylcellulose (HEC) using capillary electrophoresis. Rheological studies confirmed that the entanglement threshold (Φ^*) for the solution is *ca.* 0.003 g/ml, in good agreement with theoretical predictions. A mesh size an order of magnitude smaller than that found in agarose gels was calculated using polymer-entanglement theory and was confirmed by electrophoretic measurements. Electrophoretic migration was shown to follow the Ogston regime under most conditions. An approach for obtaining smaller mesh sizes is presented.

INTRODUCTION

It is well known that the electrophoretic mobility of double-stranded DNA (dsDNA) in free solution is not a strong function of molecular size [1,2]. Therefore, in order to effect an electrophoretic separation of dsDNA mixtures, one has had to perform the separation in a cross-linked rigid gel matrix which alters the frictional characteristics of DNA in such a way as to introduce a molecular weight dependence to its electrophoretic mobility.

However, with the advent of capillary electrophoresis (CE), superior separations of dsDNA mixtures have been demonstrated without the use of a rigid cross-linked gel matrix [3,4]. These studies demonstrate that, by using a semi-dilute, low-viscosity polymer solution as the separation medium, high-resolution separations of dsDNA mixtures can be achieved. Although electrophoresis in non-cross-linked polymer solutions has been previously demonstrated [5,6], never before has such high resolution been achieved in low-viscosity solutions. This technique promises to combine the advantages of free-solution capillary electrophoresis (system automation, speed, reproducibility and accurate quantification) with the range of application and resolving power of gel-based systems.

This paper represents an attempt to interpret these recent results using polymer entanglement concepts and traditional theories of gel electrophoresis. We also report the effect of fragment length and polymer concentration on the electrophoretic mobility of DNA fragments ranging from 118 to 1353 base pairs (bp) in solutions of

0021-9673/91/$03.50

hydroxyethylcellulose (HEC). These data are then compared with theoretical predictions.

EXPERIMENTAL

The capillary electrophoresis system used in this work closely resembles that described elsewhere [7,8]. A straight length of polyimide-coated fused-silica capillary (Polymicro Technologies, Phoenix, AZ, USA), 50 cm long (35 cm to the detector), with I.D. 50 μm and O.D. 375 μm, connects the anodic reservoir with the electrically grounded cathodic reservoir. A high-voltage power supply capable of producing up to 30 000 V (Gamma High Voltage Research, Ormand Beach, FL, USA) was used to drive the electrophoretic process. Current through the capillary was measured over a 1-kΩ resistor in the return circuit of the power supply using a digital multimeter (Model 3465B, Hewlett-Packard, Palo Alto, CA, USA). On-column UV detection at 260 nm was carried out using a modified variable-wavelength detector (Model 783, Applied Biosystems, Foster City, CA, USA). The electrophoresis system was enclosed in an insulated compartment having safety interlocks in order to prevent electric shock. Data were collected using an integrator (Model 3390A, Hewlett-Packard). Samples were introduced into the capillary by applying a vacuum of 5 inchHg (16884 Pa) to the cathodic electrode reservoir for 2–3 s while the anodic end of the capillary was immersed in the sample solution. After the sample slug had been introduced into the capillary, the anodic end of the capillary was placed back in the electrophoresis buffer together with the anodic electrode, and the electrophoretic voltage was then applied. The temperature of the agitated air surrounding the capillary was maintained at 30.0 $\pm$ 0.1°C in all experiments. A description of the methods used to calculate electrophoretic mobilities is provided elsewhere [9].

Viscosity measurements were performed using an Ostwald viscometer [10] thermostated in a water-bath at 30.0 $\pm$ 0.5°C.

The DNA mixture used was a commercially prepared restriction digest of the ΦX174 plasmid (Bethesda Research Labs., Bethesda, MD, USA). The buffer used in all experiments was 89 m*M* tris(hydroxymethyl)aminomethane (Tris)–89 m*M* boric acid–5 m*M* ethylenediaminetetraacetic acid (EDTA) with varying amounts of added hydroxyethylcellulose (HEC).

RESULTS AND DISCUSSION

Polymer entanglement

An important difference exists between polymer solutions which are dilute, where the polymer chains are hydrodynamically isolated from one another, and more concentrated solutions, where the chains overlap and interact. The polymer volume fraction at which the polymer chains begin to interact with one another, Φ^*, is the over-lap threshold. Above this concentration, the solution is said to be entangled (Fig. 1). The over-lap threshold can be estimated using a relationship derived by De Gennes [11]:

$$\Phi^* \approx N^{-\frac{4}{5}} \tag{1}$$

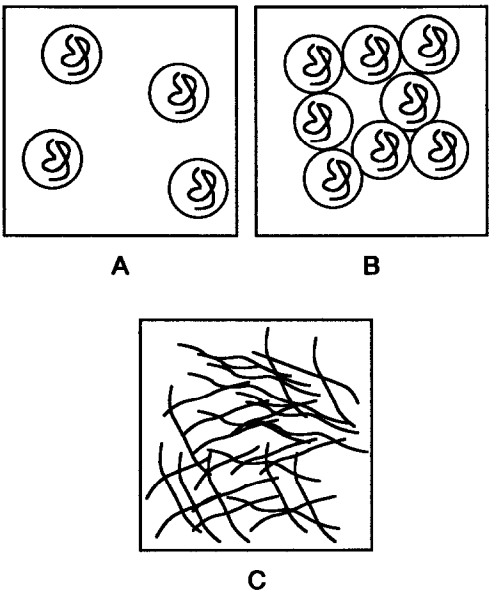

Fig. 1. Representation of the entanglement process. (A) Dilute solution where $\Phi < \Phi^*$; (B) solution at entanglement threshold where $\Phi \approx \Phi^*$; (C) fully entangled solution where $\Phi > \Phi^*$.

where N is the number of segments in the polymer chain. This expression is derived by assuming that at the over-lap threshold, Φ is the same as the local concentration inside a single coil. Eqn. 1 further assumes that the polymer is in an athermal solvent. Note that if N is large, Φ^* can be very small. For example, if $N = 10^4$, Φ^* is of the order of 10^{-3}.

Experimentally, the point at which a polymer solution becomes entangled can be determined by plotting the logarithm of the specific viscosity as a function of polymer volume fraction [12]. For independent, non-interacting polymer molecules, *i.e.*, $\Phi < \Phi^*$, dilute solution theories predict that the slope of such a curve would be *ca.* 1.0 [13]. As the polymer coils begin to interact, the slope is expected to increase. Our experimental results are presented in Fig. 2 for solutions of HEC dissolved in the electrophoresis buffer, giving $\Phi^* \approx 0.29\%$.

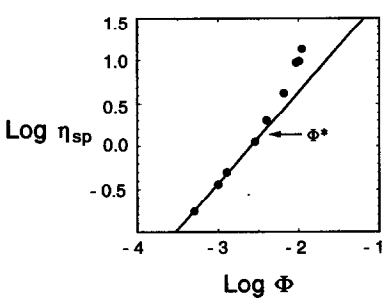

Fig. 2. Dependence of specific viscosity, η_{sp}, of HEC buffer solution on HEC volume fraction. The slope of the line passing through the first four points is 1.07, in good agreement with the value of 1.0 expected from dilute solution theories. Deviation from this line occurs at HEC concentrations between 0.0029 and 0.0040 g/ml, indicating the onset of entanglement effects in this concentration range.

To check the agreement between the experimental value of Φ^* and that predicted by eqn. 1, we must determine an approximate value for N for the HEC. This was done by the application of the Mark–Houwink–Sakurada equation using intrinsic viscosity measurements performed on aqueous solutions of HEC [14]. The measured value of the intrinsic viscosity of HEC in water, $[\eta]$, was found to be 376 ml/g. The resulting value of N is 1025, assuming a monomer molecular weight of 187. With this value of N, eqn. 1 predicts Φ^* to be 0.39%. Given the approximate nature of these scaling laws, this is in good agreement with the experimental value.

Characteristic mesh size

An entangled solution is characterized by an average mesh size for the network, ξ. The expression relating ξ to the polymer concentration is [11]

$$\xi(\Phi) \approx a\,\Phi^{-\frac{3}{4}} \tag{2}$$

where a is the length of one repeat unit along the polymer chain and $\Phi^* < \Phi < 1$. Again, eqn. 2 assumes an athermal solvent.

In order to apply eqn. 2 to calculate mesh size, we must first estimate a value for the statistical segment length, a, for HEC. The value of a can be estimated using intrinsic viscosity measurements. For a random-coil polymer [15],

$$[\eta] = \frac{\Phi_c \langle r^2 \rangle^{\frac{3}{2}}}{\mathrm{MW}} \tag{3}$$

where Φ_c is a universal constant having a value of $2.1 \cdot 10^{23}$ if $[\eta]$ has the units of ml/g and $\langle r^2 \rangle$ is the root-mean-squared end-to-end distance between the ends of the polymer chain. Further, for an unperturbed chain,

$$\langle R_g^2 \rangle = \frac{\langle r^2 \rangle}{6} \tag{4}$$

where R_g is the radius of gyration of the coil. Based on a measured value of 317 ml/g for $[\eta]$ in the electrophoresis buffer (data not shown), eqns. 3 and 4 give a value of 270 Å for R_g. Next, given the relationship between the segment length, a, and R_g for an unperturbed coil,

$$R_g = aN^{0.6} \tag{5}$$

and given that $N = 1025$, we can see that $a = 4.21$ Å. This is close to the 4.25 Å monomer segment length for HEC [14].

Using a value of 4.21 Å for a in eqn. 2 we obtain a mesh size of *ca.* 265 Å at $\Phi = 0.40\%$. Quantitative investigations of the actual mesh sizes in these solutions are in progress. Because an entangled mesh requires no specific cross-linking or gelation, a wide range of polymers may be easily adapted for these applications. Candidate polymers simply need to be water soluble and preferably uncharged. Further, in contrast to gels, polymer solutions are highly homogeneous structures.

Next we compare the mesh sizes of these polymer solutions with those of

traditional gels. Righetti *et al.* [16] developed an empirical relationship to correlate pore sizes in agarose gels with agarose concentration, yielding a relationship of the form

$$p = 140.7\ C^{-0.7} \tag{6}$$

where p is the pore size (in nm) and C is the concentration of agarose (in wt.%). Note that this empirical expression has the same form as eqn. 2. However, at a given concentration, the entangled solution produces a smaller mesh size, consistent with the fact that in a gel the polymer fibers exist as bundles, therefore leaving larger voids. Slater *et al.* [17] also arrived at a similar expression using electrophoresis data, and found an exponent of -0.75, in exact agreement with the form of eqn. 2.

Electrophoresis in a polymer network

Once the network structure of the polymer solution is understood, we address the effects of the polymer solution on electrophoresis. Two main theories describe the migration of a flexible macromolecule through a polymer network: the Ogston sieving model and the reptation model. The applicability of each depends on the size of the migrating molecule relative to the mesh size of the network.

The Ogston model [18,19] treats the polymer network as a molecular sieve. It assumes that the gel consists of a random network of interconnected pores having an average pore size ξ, and that the migrating solute behaves as an undeformable spherical particle of radius R_g. According to this model, smaller molecules migrate faster because they have access to a larger fraction of the available pores. The expression describing the migration of a solute through a polymer network according to the Ogston mechanism is

$$\mu = \mu_0 \exp[-Cb(R_g + r)^2] \tag{7}$$

or

$$\mu = \mu_0 \exp\left[-\frac{1}{4}\pi\left(\frac{R_g + r}{\xi}\right)^2\right] \tag{8}$$

where μ_0 is the free solution electrophoretic mobility, C the concentration of polymer, b a constant dependent on the concentration units chosen for C, R_g the radius of gyration of the migrating solute and r the radius of the mesh-forming polymer chain. Because they do not take into account the effects of the electric field on R_g, eqns. 7 and 8 only hold strictly for $\mu(E \rightarrow 0)$. Therefore, all mobility data presented here are extrapolated to zero field using five field strengths ranging from 400 to 40 V/cm. In eqn. 7 the term $b(r + R_g)^2$ is called the retardation coefficient, K_r.

When a long, flexible molecule travels through a polymer network where $R_g \gg \xi$, the assumption of an undeformed particle breaks down. Instead, the long molecule "snakes" through the polymer network "head first". The migrating solute is assumed to move through "tubes" formed by the gel matrix. In the limit of low electric field, the migrating DNA can still be considered an unperturbed random coil. In this

case, the reptation theory of De Gennes [20] can be used to derive the relationship between electrophoretic mobility and DNA size [21]:

$$\mu \sim \frac{1}{N_{\mathrm{DNA}}} \tag{9}$$

where N_{DNA} is the number of statistical segments in the DNA chain and $\sim$ indicates proportionality. In the case of high electric fields, one must take into account the deformation of the DNA coil caused by the electric field. In this case, the biased reptation model [22] applies, giving

$$\mu = \frac{Q}{3f}\left(\frac{1}{N_{\mathrm{DNA}}} + \frac{E'^2}{3}\right) \tag{10}$$

where Q is the charge on a DNA segment, f is the translational frictional coefficient of a DNA segment along the tube and E' is a dimensionless field strength given by

$$E' = \frac{\xi q E}{2kT} \tag{11}$$

where q is the effective charge on the portion of DNA contained in the pore, k the Boltzmann constant, E the actual field strength and T the absolute temperature (eqn. 10 is only valid when $E' < 1$). Note that eqn. 10 suggests that as N or E' becomes large, μ becomes independent of N.

According to Slater and Noolandi [19], based on both experimentation and numerical simulation, the transition from the Ogston to the reptation regime takes place when $R_g \approx 1.4\xi$.

Fig. 3 shows a representative electropherogram. Note that this separation is

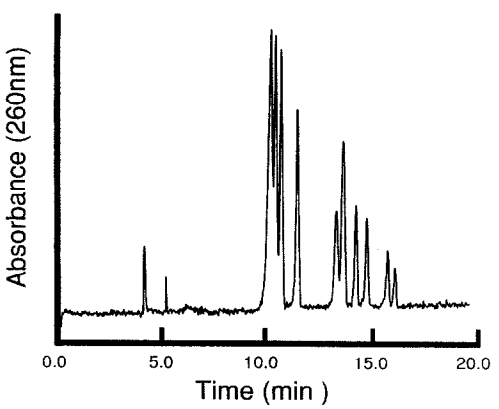

Fig. 3. Representative electropherogram showing the separation of eleven DNA restriction fragments ranging in size from 72 to 1353 bp. Reading from left to right (not including the first two peaks, which are markers) the species are 1353, 1078, 872, 603, 310, 281 + 271, 234, 194, 118 and 72 bp in length, respectively. Conditions: buffer, 0.25% HEC in 89 m*M* Tris–89 m*M* boric acid–5 m*M* EDTA; field strength, 301.3 V/cm; UV detection at 260 nm; capillary dimensions, 50 cm total length (35 cm to detector) × 50 μm I.D.; temperature, 30 ± 0.1°C.

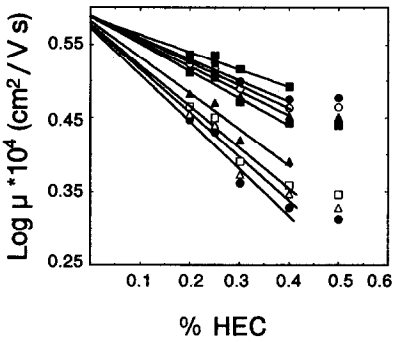

Fig. 4. Ferguson plot for sample DNA fragments. Hatched squares = 118 bp; closed circles = 194 bp; open circles = 234 bp; hatched triangles = 281 bp; closed squares = 310 bp; closed triangles = 603 bp; open squares = 872 bp; open triangles = 1078 bp; hatched circles = 1353 p. All mobility data have been extrapolated to $E = 0$.

performed slightly below Φ^*. The fact that a mesh exists at $\Phi < \Phi^*$ is probably due to the broad molecular weight distribution of the HEC, allowing larger coils to overlap below Φ^*.

According to the Ogston model, a plot of log μ *vs.* % HEC (a Ferguson plot) should give a linear relationship with a slope equal to K_r and an intercept on the ordinate equal to log μ_0. For fragments 118, 194, 234, 281 and 310 bp in solutions up to 0.4% HEC, this behavior is indeed observed (Fig. 4). The intercept for these five lines, 0.588 [relative standard deviation (R.S.D.) = 0.15%], implies a value for μ_0 of $3.87 \cdot 10^{-4}$ cm^2/V · s, in complete agreement with the measured electrophoretic mobility of these fragments at 0% HEC of $3.86 \cdot 10^{-4}$ cm^2/V · s (R.S.D. = 1.2%, $n = 16$). For fragments larger than 310 bp, the agreement degrades. This is probably due to the gradual transition to the reptation regime for these larger fragments. This transition has also been observed in agarose gels [23]. According to the Ogston model, a plot of $K_r^{0.5}$ *vs.* R_g should yield a linear relationship. As seen in Fig. 5, for the smaller fragments, agreement with the prediction of the Ogston model is close, whereas the larger fragments deviate significantly. Assuming that the Ogston–reptation transition

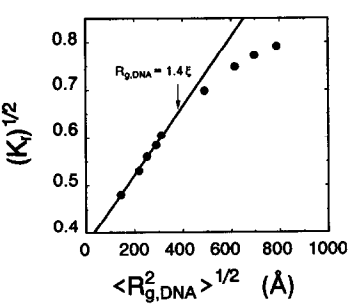

Fig. 5. Square root of the retardation coefficient K_r *vs.* the root-mean-square radius of gyration $\langle R_g^2 \rangle^{1/2}$ of the DNA fragments. $\langle R_g^2 \rangle^{1/2}$ is calculated for DNA using the Porod–Kratky stiff-chain model assuming a persistence length of 450 Å and a contour length of 3.4 Å per base pair [24]. All mobility data have been extrapolated to $E = 0$.

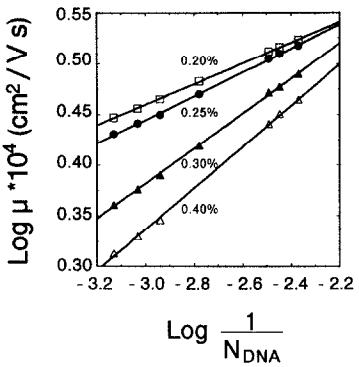

Fig. 6. Logarithm of the electrophoretic mobility *vs.* logarithm of inverse molecular size (in base pairs) for different HEC concentrations. A slope of 1 would be expected if migration exactly followed the reptation mechanism. (□) 0.20% HEC, slope = 0.091; (●) 0.25% HEC, slope = 0.107; (▲) 0.30% HEC, slope = 0.158; (△) 0.50% HEC, slope = 0.201. All mobility data have been extrapolated to $E = 0$.

occurs when $R_g \approx 1.4\xi$, Fig. 5 implies that for HEC at 0.4% in this buffer, 223 Å < ξ < 350 Å. This value for ξ agrees with the mesh size predicted from eqn. 2 (ξ = 265 Å at 0.40% HEC).

Fig. 6 shows log μ as a function of $1/N_{DNA}$. According to eqn. 10, these curves should be linear with slopes of 1.0 if the fragments migrate by the reptation mechanism. As expected from the previous analysis, for the conditions used in these experiments none of the curves adheres to the reptation behavior. However, as the HEC concentration is increased, the slopes of the curves appear to increase towards 1, indicating a transition regime. Again, this behavior has been observed for low-concentration agarose gels using small DNA fragments [23].

It is likely that once $R_g \gg \xi$, *i.e.*, when reptation becomes important, the separation performance of these systems will decrease rapidly. This is because at the high electrical fields typically employed in capillary electrophoresis, the value of E' in eqn. 10 is greater than 1, resulting in a saturated, size-independent mobility [19]. Although this limitation is not unique to the polymer solution system, it does represent a restriction on the ability to exploit the high electric fields and thus enjoy the consequent rapid analysis using CE. In order to overcome this limitation, high-voltage pulsed-field techniques will need to be investigated, a topic currently under investigation.

For some applications, smaller mesh sizes that those used here may be required. Ideally, one would like to maintain the advantages of a low-viscosity solution when going to a smaller mesh. The above relationships give an indication of how this might be accomplished. As can be seen from Fig. 2, in order to minimize the viscosity of the polymer solution, one wants to operate near Φ^*. However, eqn. 2 predicts that, in order to achieve a small mesh, one needs a large Φ. To satisfy both constraints, one must use a short polymer to form the mesh. This can be demonstrated by combining eqns. 1 and 2 to give the expression

$$\xi\,(\Phi^*) \approx aN^{0.6} \tag{12}$$

Therefore, in order to create larger pores one wants to use a longer polymer and in order to create smaller pores one wants to use a shorter polymer.

The application of entangled polymer solutions as a "sieving" medium has also been exploited by Langevin and Rondelez [25] in the context of centrifugation. This work is a direct analogue to electrophoresis in entangled solutions.

CONCLUSIONS

It appears that low-viscosity polymer solutions provide a good matrix for electrophoretic separations. By performing polymer solution electrophoresis in a capillary, one has in effect decoupled the two roles of a traditional electrophoresis gel: that of a sieving matrix and that of an anti-convective stabilizing medium. Separations of short DNA fragments appear to follow the Ogston model in a manner similar to that found in agarose gel systems. At present, using high electrical fields, separations will be limited to the Ogston regime until pulsed-field techniques are invoked. Also, simple relationships from entangled polymer network theories can be used to guide the further development of these systems.

ACKNOWLEDGEMENTS

The financial support of the University of California at Berkeley BRSG Fund and a generous research grant from Applied Biosystems are greatly appreciated. We thank A. M. Chin, D. S. Nelson and J. C. Colbum for helpful comments and discussions and S. V. Patel for invaluable assistance in performing the experimental work.

REFERENCES

1 B. M. Olivera, P. Baine and N. Davidson, *Biopolymers*, 2 (1964) 245.
2 J. J. Hermans, *J. Polym. Sci.*, 18 (1953) 257.
3 A. M. Chin and J. C. Colburn, *Am. Biotech. Lab. News Ed.*, 7 (1989) 10A.
4 M. Zhu, D. L. Hansen, S. Burd and F. Gannon, *J. Chromatogr.*, 480 (1989) 311.
5 D. Tietz, M. H. Gottlieb, J. S. Fawcett and A. Chrambach, *Electrophoresis*, 7 (1986) 217.
6 D. N. Heiger, A. S. Cohen and B. L. Karger, *J. Chromatogr.*, 516 (1990) 33.
7 J. N. Jorgenson and K. D. Lukacs, *Science*, 222 (1983) 266.
8 H. H. Lauer and D. McManigill, *Anal. Chem.*, 58 (1986) 166.
9 P. D. Grossman, J. C. Colburn and H. H. Lauer, *Anal. Biochem.*, 179 (1989) 28.
10 F. Rodriguez, *Principles of Polymer Systems*, McGraw Hill, New York, 1982, Ch. 7.
11 P. G. De Gennes, *Scaling Concepts in Polymer Physics*, Cornell University Press, Ithaca, NY, 1979, Ch. 3.
12 D. A. Hill and D. S. Soane, *J. Polym. Sci. Polym. Phys. Ed.*, B27 (1989) 2295.
13 H. R. Allcock and F. W. Lampe, *Contemporary Polymer Chemistry*, Prentice-Hall, Englewood Cliffs, NJ, 1981, Ch. 15.
14 J. Brandrup and E. H. Immerut (Editors), *Polymer Handbook*, Wiley, New York, 3rd ed., 1989, Ch. 7.
15 P. J. Flory, *Principles of Polymer Chemistry*, Cornell University Press, Ithaca, NY, 1953.
16 P. G. Righetti, B. C. W. Brost and R. S. Snyder, *J. Biochem. Biophys. Methods*, 4 (1981) 347.
17 G. W. Slater, J. Rousseau, J. Noolandi, C. Turmel and M. Lalande, *Biopolymers*, 27 (1988) 509.
18 A. G. Ogston, *Trans. Faraday Soc.*, 54 (1958) 1754.
19 G. W. Slater and J. Noolandi, *Biopolymers*, 28 (1989) 1781.
20 P. G. De Gennes, *J. Chem. Phys.*, 55 (1971) 572.
21 L. S. Lerman and H. L. Frisch, *Biopolymers*, 21 (1982) 995.

22 O. J. Lumpkin, P. Dejardin and B. H. Zimm, *Biopolymers*, 21 (1985) 1573.
23 H. Hervet and C. P. Bean, *Biopolymers*, 26 (1987) 727.
24 C. R. Cantor and P. R. Schimmel, *Biophysical Chemistry*, Freeman, New York, 1980, Ch. 19.
25 D. Langevin and F. Rondelez, *Polymer*, 19 (1978) 875.